Article

Preparation, Characterization, DFT Calculations, Antibacterial and Molecular Docking Study of Co(II), Cu(II), and Zn(II) Mixed Ligand Complexes

Maged S. Al-Fakeh [1,2,*], Sabri Messaoudi [1,3], Faisal I. Alresheedi [4], Abuzar EAE Albadri [1], Wael A. El-Sayed [1,5] and Emran Eisa Saleh [6,7]

1 Department of Chemistry, College of Science, Qassim University, Buraidah 51452, Saudi Arabia, m.alfakeh@qu.edu.sa
2 Taiz University, Taiz 3086, Yemen,
3 Carthage University, Faculty of Sciences of Bizerte, 7021 Jarzouna, Tunisia, s.messaoudi@qu.edu.sa
4 Department of Physics, College of Science, Qassim University, Buraidah 51452, Saudi Arabia, falresheedi@qu.edu.sa
5 Photochemistry Department, National Research Centre, Cairo 12311, Egypt, wshendy@qu.edu.sa
6 Physics Department, Faculty of Science, University of Aden, Yemen, esas.2009@yahoo.com
7 Physics Dep., Faculty of Science, Ain Shams University, Egypt.
* Correspondence: m.alfakeh@qu.edu.sa

Abstract: [Co(AMPY)(DAPY)Cl2(H2O)].H2O (1) [Cu(AMPY)(DAPY)Cl2(H2O)].H2O (2) [Zn(AMPY)(DAPY)Cl2(H2O)] (3) were prepared from the ligands; AMPY = 2-amino-4-methylpyrimidine (L1), DAPY = 2,3-diaminopyridine (L2) and CoCl2.6H2O, CuCl2.2H2O and ZnCl2 in water/ethanol solutions and the three products characterized by elemental analysis, ultraviolet-visible spectroscopy (UV–Vis), Fourier-transform infrared spectroscopy (FT-IR), magnetic susceptibility, molar conductivity methods, and TGA analysis. The X-ray powder diffraction of the Co(II), Cu(II), and Zn(II) compounds showed that the geometry of monoclinic and SEM analysis revealed their morphology with a smooth surface. Molecular modeling was performed for all compounds using the density functional method DFT/B3LYP to study the structures and the frontier molecular orbitals (HOMO and LUMO). We have used Gaussian09 software for the calculations. In this study, different complexes were tested against Gram negative and Gram positive bacterial species to give insight into their broad-spectrum effects. The used pathogenic strains were two Gram positive species "Staphylococcus aureus and Micrococcus luteus" and two Gram negative species "Salmonella thyphimurium and Escherichia coli. The antifungal activity was evaluated against a pathogenic reference strain of the yeast Candida albicans. The antimicrobial and antioxidant assay results demonstrate that the tested compounds are effective against Gram positive and negative bacteria. Additionally, the compounds have an antifungal effect against Candida albicans with a maximum inhibitory zone of 2.5cm. The results demonstrated high antioxidant potential for the Zn(II) complex with a DPPH scavenging of 91.5%, however, the Cu(II) complex was low (16.5%). The data of docking with tyrosyl-tRNA synthetase presented that all compounds fit very well in the catalytic pockets of the proteins of the receptor.

Keywords: Mixed-Ligands; DFT Calculations; HOMO; LUMO; Antimicrobial; Antioxidant Assays; and Molecular Docking Analysis

1. Introduction

Transition element ions (TEI) have a good and important role in the self-assembly of complexes. Additionally, the wide field of chemistry using transition elements and organic ligands as building blocks is enriched with high design ability and a variety of structural architecture [1-4]. The cobalt(II), copper(II), and zinc(II) ions are of particular interest because it relates to labile metal centers with the coordination number of M2+ from two

Preprints (www.preprints.org) | NOT PEER-REVIEWED | Posted: 19 December 2022 doi:10.20944/preprints202212.0329.v1

to six and more. Co(II), Cu(II), and Zn(II) compounds are most commonly given with nitrogen-containing ligands with functional groups and different geometries. Such as pyridine, pyrimidine, and its derivatives react with metal ions (MIS) to give bothpolynuclearr and discrete coordination compounds and participate in hydrogen-bonding and π-ring including weak interactions as well as coordinates to the transition element [5-7]. Moreover, it has an immense influence on various biological and chemical processes as well [8]. We have observed this through antimicrobial and antioxidant assays of the prepared compounds. 2-amino-4-methylpyrimidine and 2,3-di-aminopyridine serve as useful chelating ligands in a diversity of inorganic, organometallic applications and anti-bacterial, anti-fungal, antioxidant, anti-inflammatory, and pharmaceutical applications [9-15]. The chemistry of Co(II), copper(II), and zinc(II) compounds with nitrogen donor ligands, especially with aminopyridine and aminopyrimidine derivatives, has been studied extensively, over the past few decades [16-17]. In this study, we prepared the three complexes $[Co(AMPY)(DAPY)Cl_2(H_2O)].H_2O$, $[Cu(AMPY)(DAPY)Cl_2(H_2O)].H_2O$ and $[Zn(AMPY)(DAPY)Cl_2(H_2O)]$. The structures of three compounds have been proposed by assessing the data obtained from (C.H.N), (FTIR), (UV-Vis), X-ray powder diffraction, molar conductivity, magnetic susceptibility methods, and molecular docking analysis. The structures of the ligands are presented in Fig. 1.

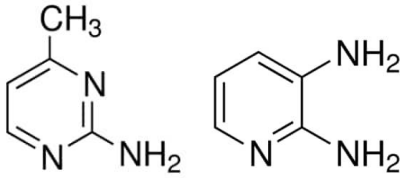

Figure 1. The structures of the ligands.

2. Experimental

2.1. Materials and Physical Measurements for Complexes

High purity 2-amino-4-methylpyrimidine (97%) and 2,3-diaminopyridine (95%) were supplied from Sigma Aldrich grade. They were purchased and used without purification. Carbon, hydrogen, and nitrogen were carried out by using the Analyischer Functions, The elemental analyzers were determined using a Gmbh Vario El analyzer, structural information was obtained from FT-IR spectra on a Thermo Nicolet (6700) FT-IR spectrophotometer, with a wavenumber range of 400-4000cm^{-1}, and UV-vis absorption was recorded on a UV–2102 PC Shimadzu using a 1 cm matched quartz cuvette in the wavelength range of 200 to 900 nanometers. At room temperature, magnetic susceptibility was used to measure the complexes using a magnetic susceptibility balance from MSB–Auto. Thermogravimetry analysis (TGA) and differential thermal analysis (DTA) were conducted in air atmosphere on a Shimadzu DTG 60 thermal analyzer, at a heating rate 10C min^{-1}. Measurements of the X-ray diffraction (XRD) were carried out using an XRD diffractometer Model (PW 1710) (Cu-Kα radiation). The morphology and structure of the synthesized materials were characterized using a scanning electron microscope, JEOL/JEM 1010 High-Resolution SEM [18].

2.2. Microbial strains and culture media

In this study, different samples were tested against Gram (–ve) and Gram (+ve) bacterial strains, giving insight into their broad-spectrum effect. The used pathogenic species were two Gram-positive strains "*Staphylococcus aureus* ATCC 25923 **(S1)** and *Micrococcus luteus* NCIMB 8166 **(S4)**" and two Gram negative strains " *Escherichia coli* ATCC 35218 **(S5)** and *Salmonella thyphimurium* ATCC 14028 **(S10)**. The antifungal activity was evaluated against a pathogenic reference strain of the yeast *Candida albicans* ATCC 90028 **(9C).** The species were grown in nutrient broth (Oxoid) at 37°C for a day and cultivated on nutrient agar (Oxoid) for 24 h at 37°C. The yeast strain was grown in Sabouraud Chloramphenicol

Preprints (www.preprints.org) | NOT PEER-REVIEWED | Posted: 19 December 2022 doi:10.20944/preprints202212.0329.v1

broth (Oxoid) at 25◦C for a day and cultivated on Sabouraud Chloramphenicol agar(Oxoid) for 24h at 37°C. The different strains are recorded in Table 1.

Table 1. The used microbial strains.

Strain	Reference
Gram positive bacteria	
S1	*Staphylococcus aureus* ATCC 25923
S4	*Micrococcus luteus* NCIMB 8166
Gram negative bacteria	
S5	*Escherichia coli* ATCC 35218
S10	*Salmonella thyphimurium* ATCC 14028
Yeast	
9C	*Candida albicans* ATCC 90028

2.3. Antimicrobial activity

The antimicrobial activity of the different extracts was tested with the reference agar disk diffusion method [19]. Before the test, 50mg of each extract were dissolved in 1 ml of a solution of dimethylsulfoxyde "DMSO" (5%). The species were grown in Mueller–Hinton broth (Oxoid) at 37°C for a day at 37°C for 24 h and the suspensions were checked with 0.5 McFarland standard turbidity. Afterward, 100µl of each precultured suspension was spread onto plates containing MH agar. Sterile filter paper discs (6mm in diameter) were saturated with 20µl of the different compounds and placed on agar. The treated plates were putted for 60 minutes at 4 °C and then incubated for a day at 37°C. Then incubation, the diameter of the inhibition zone (clear halo) about the discs was measured.

2.4. Antioxidant Activity

(DPPH) Radical Scavenging Assay

The free radical scavenging effect of the compounds was assessed according to the method [20]. Briefly, 1 mL of sample (5mg/mL) was mixed with 3mL of methanolic solution of DPPH (2,2-diphenyl-1-picrylhydrazyl) (300 µM). The reaction mixture was vortexed and incubated for 30min at room temperature. The absorbance of the sol. was measured at 517nanometers. Vitamin C was used as a standard. The inhibitory percentage of (DPPH) was measured by using the next equation (1):

(DPPH) Scavenging effect (%) = [1- (Abs compound/Abs control)] × 100

2.5. Computational studies

The density functional theory (DFT) was performed by using Gaussian09 program [21]. The optimization of the diverse complexes was done by DFT through the functional B3LYP and Lanl2dz/6-31G(d) basis sets. LANL2DZ basis set was limited for the treatment Zn(II), Cu(II), and Co(II) atoms and 6-31G(d) basis set for all other atoms. To confirm the stability of the structures, we calculated the vibrational frequencies at the same level of theory

2.6. Molecular Docking Analysis

In silico molecular docking was used to study the interactions between S. aureus tyrosyl-tRNA synthetase and the three complexes Co(II), Cu(II), and Zn(II) to investigate the preferred occupation of the ligands in the binding active site. The crystal coordinates were got from the Protein Data Bank: S. aureus, tyrosyl-tRNA synthetase (PDB: 1JIJ). All water species and the co-crystallized ligand have been deleted from the original structure. We designated Gasteiger charge and polar hydrogens using AutoDockTools1.5.2 (ADT) and we prepared the PDBQT file format [22]. We used ADT to determine a docking grid. In 1JIJ, the grid box site was set at x: −10.908,y : 14.432 y, and z : 86.420 z Å. The size of the grid box size was 25 Å for x, y, and z, and 0.375 Å for the grid spacing. The structures of

Preprints (www.preprints.org) | NOT PEER-REVIEWED | Posted: 19 December 2022 doi:10.20944/preprints202212.0329.v1

the compounds were those optimized in computational studies with B3LYP/LanL2dz/6-31G(d). We used AutoDock Vina software [23] with 32 as an exhaustiveness parameter to get the docking data. The docking conformation analysis was done by ADT. Enzyme ligand interactions are investigated by Discovery Studio Visualizer [24].

2.7. Synthesis of three metal mixed ligand complexes

2.7.1. [Co(AMPY)(DAPY)Cl_2(H_2O)].H_2O (1)

A ethanolic solution (15mL) of 2-Amino-4-methylpyrimidine (AMPY) (0.5g, 0.45mmol) was slowly added into 20mL water of $CoCl_2.6H_2O$ (1.09g, 0.45mmol) and to it a ethanolic solution (15mL) of 2,3-diaminopyridine (DAPY) (0.5g, 0.45mmol) was added dropwise. The reaction mixture was heated at 60°C for 60 minutes with constant stirring. The dark brown precipitate was washed with H_2O and EtOH and then dried.

2.7.2. [Cu(AMPY)(DAPY)Cl_2(H_2O)].H_2O (2)

It was prepared adopting the same procedure as in the case of (1). The molar ratio was 1:1:1, $CuCl_2.2H_2O$ (0.78g, 0.45mmol), AMPY (0.5g, 0.45mmol) and DAPY (0.5g, 0.45mmol). A dark green complex was isolated.

2.7.3. [Zn(AMPY)(DAPY)Cl_2(H_2O)] (3)

A similar synthetic method as that for (**1**) was used in the prepared zinc(II) complex (15mL), $ZnCl_2$ (0.62g, 0.45mmol). A creamy white compound was obtained.

3. Results And Discussion

3.1. Synthesis and Spectroscopic Characterization

Co(II), Cu(II), and Zn(II) compounds were synthesized in aqueous media using cobalt(II) chloride hexahydrates, copper(II) chloride dehydrated and zinc(II) chloride salts and 2-Amino-4-methylpyrimidine (AMPY) as primary ligands. 2,3-diaminopyridine (DAPY) was used as the auxiliary ligand for the three complexes, respectively. Details of the preparation procedure are presented in the experimental part. Fourier Transform infrared (FT-IR) spectra in (Figure 1). These components were found to react in the molar ratio 1: 1: 1 metal : L1 : L2. The compounds are air stable. The molar conductivity values ΛM of the compounds in 10^{-3} M DMSO solutions vary from 23.2, 38.8 to 62.1 S cm^2 mol^{-1} for Zn(II), Cu(II), and Co(II) complexes respectively.

Anal. Calc. for $C_{10}H_{18}N_6CoCl_2O_2$ (**complex 1**): C, 31.22; H, 4.71; N, 21.87; Found: C, 32.04; H, 4.56; N, 20.98. m.p. 198 °C.

Anal. Calc. for $C_{10}H_{18}N_6CuCl_2O_2$ (**complex 2**): C, 30.89; H, 4.66; N, 21.61. Found: C, 30.46; H, 4.28; N, 21.04. m.p. 192 °C.

Anal. Calc. for $C_{10}H_{16}N_6ZnCl_2O$ (**complex 3**): C, 32.23; H, 4.32; N, 22.55. Found: C, 33.50; H, 4.11; N, 21.96. m.p. 186 °C.

3.2. Fourier Transform Infrared Spectra

The infrared spectral bands provide structural evidence for the coordination of the two ligands to the Co(II), Cu(II), and Zn(II) ions. The assignment of the most characteristic FT-IR bands of the three compounds is shown in table (2) together with those of the two ligands listed for comparative purposes and to facilitate the spectral data. The stretching vibration of the pyridine groups located at 1590 (ν) C=C and 1580 (ν) C=N cm^{-1} in the DAPY ligand exhibits a notable shift to a wave number (1548-1567) and (1530-1540cm^{-1}) in all complexes [25-27]. The C-N stretching in the ring bands found in the complexes are in the range 1450-1495 cm^{-1} [28]. In the IR spectrum of the free AMPY, υ(C-NH_2) occurs at 3312cm^{-1} with a shift to a wave number (3296-3310 cm^{-1}) in the spectra of the compounds [8]. A broad diffused band with medium intensity located in the range 3418-3498 cm^{-1} may be assigned to ν(OH) for lattice H_2O in Co(II) and Cu(II) complexes [29]. For all complexes, the νOH stretching vibration of coordinated H_2O appears at the 3306-3326cm^{-1} region [30].

Preprints (www.preprints.org) | NOT PEER-REVIEWED | Posted: 19 December 2022 doi:10.20944/preprints202212.0329.v1

The IR spectra of the compounds appear as a band at 418-436 cm^{-1} assigned to (M-Cl) [31]. Metal-oxygen and M-nitrogen bonding are apparented by the manifestation of two bands at 554-570 and 468-475cm^{-1} district, respectively [32].

Table 2. The infrared spectral data (cm^{-1}) of the ligand and their complexes.

Assignment	AMPY	DAPY	Co(II) complex	Cu(II) complex	Zn(II) complex
υO-H lattice water	-	-	3498	3418	-
υO-H coordinated water			3326	3306	3307
υNH_2	3312	-	3310	3296	3302
υN-H	-	3179	3132	3160	3172
υCH_3	2920w	-	2928	2932	2930
υC-H	3006m	-	2998w	2994w	2988w
υC=C	-	1590	1548	1555	1567
υC=N	-	1580	1536	1530	1540
$\upsilon C\text{-}N_{\text{in ring}}$	-	1456	1450	1482	1495
υC-H		742	748	760	750
M-O	-	-	554	570	556
M-N	-	-	468	472	475
M-Cl	-	-	418	436	428

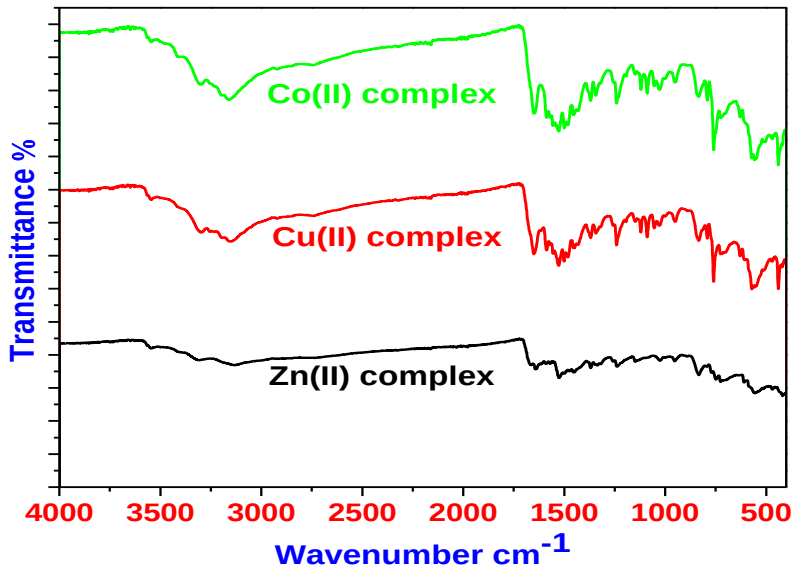

Figure 2. FT-IR of the Co(II), Cu(II) and Zn(II) complexes.

3.3. Magnetic Moments

Magnetic susceptibility was measured at room temperature using a solid sample by Gouy operation. The magnetic moment shows the Co(II) ion to be (4.78 BM) with configuration in an octahedral environment [33,34]. The value of the determined magnetic moment for Cu(II) ion is (1.73 B.M.) based on the configuration in octahedral geometry [35,36]. Zn(II) is a nonmagnetic ion. The value for Co is between 4.3 and 5.2, so it is in the high spin state

3.4. Electronic Spectra

In the wavelength range 200-650 nm, the optical absorption coefficient was calculated" for ligands (DMSO, 1×10-3 M) and their metal ions (Co(II), Cu (II), and Zn(II)) as shown in figure (3) below. Absorption peaks were found at 31,746, 31,250, 32,476cm-1 and 39,682, 39,062, 39.370cm-1, which can be referred to as the n-π*, π-π*, transition of DAPY

Preprints (www.preprints.org) | NOT PEER-REVIEWED | Posted: 19 December 2022 doi:10.20944/preprints202212.0329.v1

and AMPY [37,38]. The electronic spectra of the cobalt(II) complex have two absorption bands "typical of high spin and low spin octahedral geometries designated to 4 T1g(F)→4 A2g(F) and 2 Eg→2 T1g transitions respectively [34]. The Cu(II) complex presented the absorption bands that need theoretical calculations in order to determine its coordination number. Zn^{+2} is a nonmagnetic ion. They have only bands for π-π*and n-π*, which are assigned to intra-ligand charge-transfer transitions. From the previous data [elemental analysis, infrared and electronic spectra, magnetic moment measurements, and molar conductance measurements, we can propose the following chemical formulae for the synthesized three metal mixed ligand complexes. (Fig.4,5).

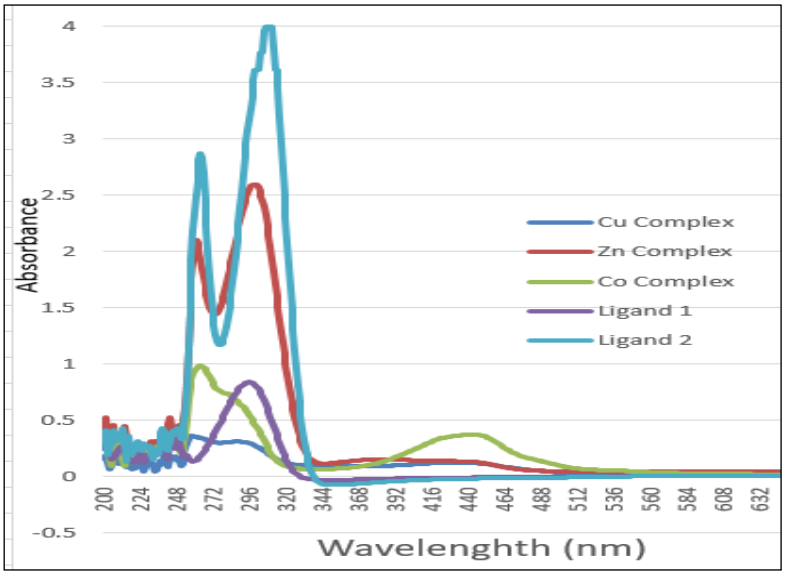

Figure 3. Electronic spectra of L1, L2, Co(II) Cu(II) and Zn(II) mixed ligand complexes.

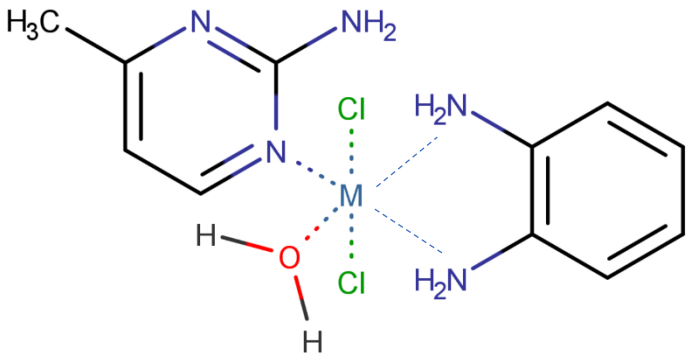

Figure 4. Structure of [M(AMPY)(DAPY)Cl_2(H_2O)].nH_2O.

M = Co(II), Cu(II) and Zn(II), n = 0 or 1 H_2O.

Preprints (www.preprints.org) | NOT PEER-REVIEWED | Posted: 19 December 2022 doi:10.20944/preprints202212.0329.v1

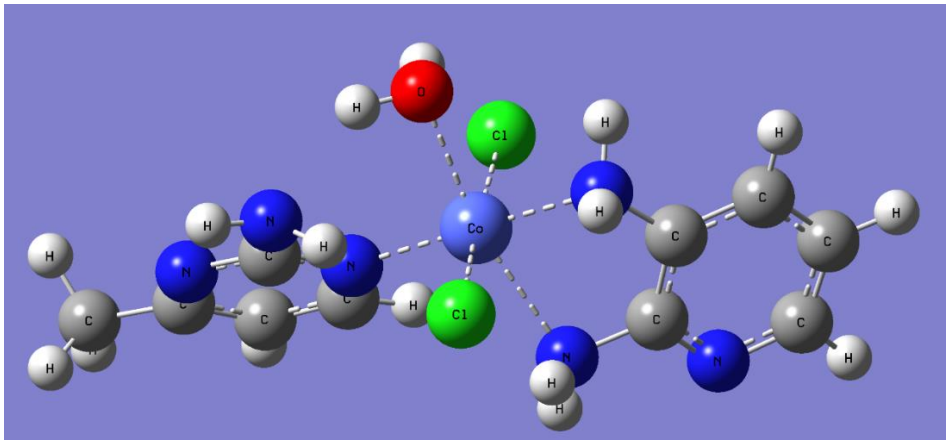

Figure 5. A perspective view of the complete coordination around Co(II) complex.

3.5. Theoretical study

Molecular modeling was performed for all compounds using the density functional theory DFT/B3LYP to study the structures (Figure 6) and the frontier molecular orbitals (Figure 7). The mode of bonding is pentacoordinate for Cu and hexacoordinate for Zn and Co. Selected bond lengths (Å) calculated at B3LYP are presented in table (3). Zn is coordinated to one nitrogen of L1 (Zn-N = 2.10Å) and to two nitrogen's of L2 (2.28 and 2.38Å). Co is coordinated to one nitrogen of L1 (Co-N = 2.00Å) and to two nitrogen's of L2 (2.00 and 2.37Å). Cu is bonded to one nitrogen of L1 (Cu-N = 2.10Å) and one nitrogen of L2 (2.00Å). Generally, the proposed model for metals is hexacoordinate, but density functional calculations show that the copper in our environment is pentacoordinate. In the literature, we find that copper can be pentacoordinate to some ligands [39].

The HOMO and LUMO frontier orbitals are exhibited in Fig. 7. For Cu, The HOMO is localized on L2 and the LUMO is centralized on the second Ligand L1. For Zn, the HOMO is localized on one chloride and the LUMO is localized on L1. For Co, both HOMO and LUMO are found with the metal and two chlorides. This shows that the electron distribution is not the same for all molecules and this can lead to different properties [21]. For Cu which is pentacoordinate, the electron distribution is small on the chloride, but for Zn and Co, the electron density is higher at least one of the chlorides in the HOMO.

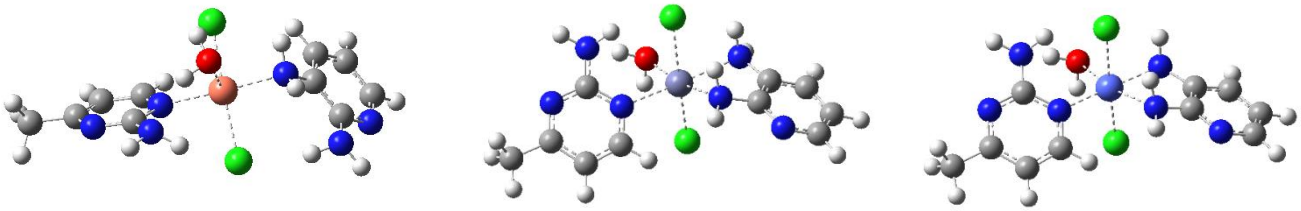

(a) $CuCl_2L1L2.H_2O$ **(b) $ZnCl_2L1L2.H_2O$** **(c) $CoCl_2L1L2.H_2O$**

Figure 6. Optimized geometry of the complexes. (a) Cu(II) (b) Zn(II), and (c) Co(II).

Table 3. Selected bond lengths (Å) calculated at B3LYP.

Bond	M = Cu	M = Zn	M = Co

Preprints (www.preprints.org) | NOT PEER-REVIEWED | Posted: 19 December 2022 doi:10.20944/preprints202212.0329.v1

M-N(L1)	2.10	2.27	2.00
M-N(L2)	2.07	2.28	2.00
M-N(L2)	-	2.38	2.37
M-Cl	2.38	2.38	2.41

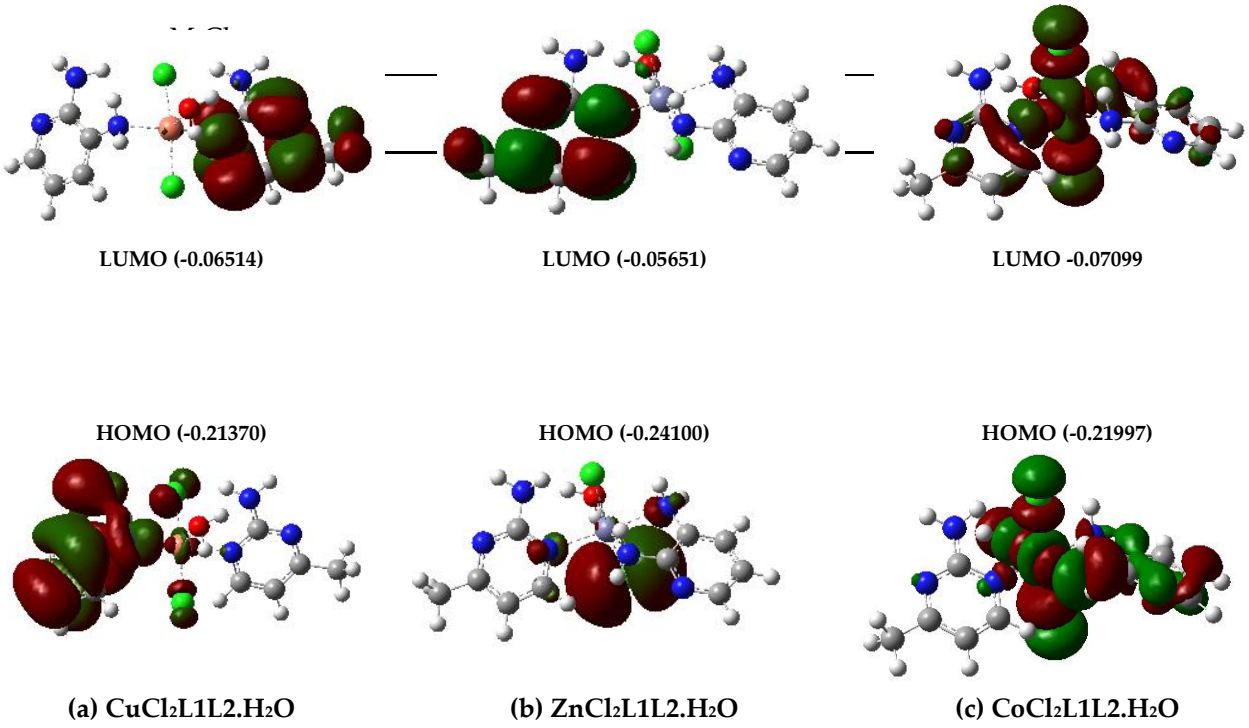

Figure 7. Frontier molecular orbitals of HOMO and LUMO of complexes. with (a) Cu (b) Zn and (c) Co.

3.6. Thermal analysis

3.6.1. $[Co(AMPY)(DAPY)Cl_2(H_2O)].H_2O$ (1)

The T.G, D.T.G, and D.T.A curves of this complex are in dynamic air. They show that the thermal decomposition processes of the compound consist of four stages. The first stage is a dehydration process occurring in the temperature range 65 to 152°C. The mass loss (calc. 9.38%, found 8.75%) indicates the loss of $2H_2O$ molecules. For this step (DTG minimum at 98°C) and an endothermic peak is observed in the DTA curve at 101°C.

$$[Co(AMPY)(DAPY)Cl_2(H_2O)].H_2O \xrightarrow{65\text{-}152^\circ C} [Co(AMPY)(DAPY)Cl_2] + 2H_2O$$

The observed mass loss of the second step (154-230°C) in the TG curve agrees with the loss of chlorine (calc. 18.45%, found 17.84%) (DTG peak at 192 °C). This step is marked on the DTA curve by an broad exothermic peak at 194 °C.

$$[Co(AMPY)(DAPY)Cl_2] \xrightarrow{154\text{-}230^\circ C} [Co(AMPY)(DAPY)] + Cl_2$$

The third and forth step (232-500°C) corresponded to the loss of decomposition of the rest organic ligands (calc. 56.81%, found 54.48%). For these steps, DTG broad minimum at 298 and 310 °C and a DTA exotherm peak at 301 and 312°C were observed. At about 550 °C, the thermal decomposition finishes and the final stable residue may be due to the formation of cobalt oxide. CoO should give a residue of 19.50%, but still 18.93% remains.

Preprints (www.preprints.org) | NOT PEER-REVIEWED | Posted: 19 December 2022 doi:10.20944/preprints202212.0329.v1

[Co(AMPY)(DAPY)]

232-500°C

CoO + decomposition product

3.6.2. $[Cu(AMPY)(DAPY)Cl_2(H_2O)].H_2O$ (2)

In dynamic air, the $[Cu(AMPY)(DAPY)Cl_2(H_2O)].H_2O$ is stable up to 88°C (Fig. 8), when a first mass loss (calc. 9.27%, found 9.02%) occurs. Correspondingly, a DTG peak at 101°C, and an endothermic broad peak at 103°C in the D.T.A curve were recorded. The observed mass loss of this first stage agrees well with the loss of two water molecules. The observed mass loss of the second step is associated with the loss of chlorine (calc. 18.23%, found 17.95%). This step corresponds to a DTG peak at 202°C and an exothermic D.T.A peak at 204°C. The third, fourth, and fifth steps of mass loss of AMPY and DAPY ligands (calc. 56.14%, found 53.16%) is manifested on the DTG curve as a peak at 251, 306, and 404 °C and an exothermic peak at 253, 308, and 406°C in the DTA curve. The end product at 550°C is consistent with CuO (calc. 20.46%, found 19.87%).

3.6.3. $[Zn(AMPY)(DAPY)Cl_2(H_2O)]$ (3)

Five-step decompositions were observed in the thermo-gravimetric curve of $[Zn(AMPY)(DAPY)Cl_2(H_2O)]$. This occurs in the temperature ranges 82-112, 114-165, 167-268, 270-335, and 337-550°C. The first mass loss (calc. 4.83%, found 4.49%) corresponds to the release of a water molecule with DTG peak at 96°C, and an endothermic peak broad at 98°C in the D.T.A curve. The observed weight loss of the second and third steps are correlated with the decomposition of AMPY and chlorine (calc. 48.32%, found 47.65%) (DTG peaks at 138 and 216°C. DTA peaks at 140 and 218°C). The fourth and fifth steps represent the decomposition of the remaining ligands (calc. 29.29%, found 27.10%). The final stable residue is ZnO (calc.21.84%, found 20.76%).

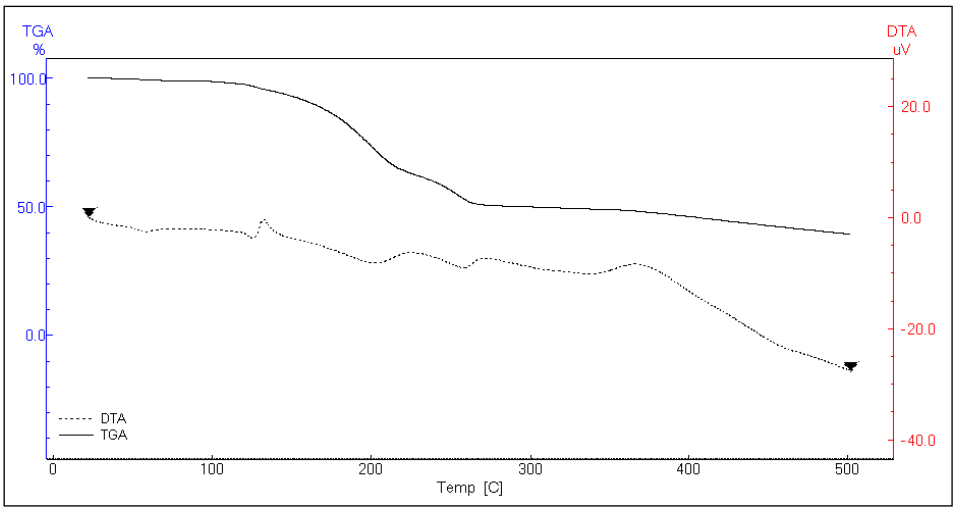

Figure 8. TG, DTG, and DTA thermograms of Cu(II) complex.

3.7. X-Ray Powder Diffraction (XRD)

The XRD patterns of chemical-synthesized complexes as shown in figures (9-10) were obtained "between the 2θ region starting from 20◦ to 80◦ ". Figures explain the crystallographic structures, whereas the atoms were arranged in the octahedral status. These XRD spectra of the complexes indicate the number of prominent diffraction peaks at particular angles. The crystallite size increases with the increase in peak intensity, directly proportional and inversely proportional to the full width at half maxima (FWHM). The protruding peaks were used to calculate the grain size via the Scherrer equation. The sharp XRD

Preprints (www.preprints.org) | NOT PEER-REVIEWED | Posted: 19 December 2022 doi:10.20944/preprints202212.0329.v1

peaks indicate that the particles were polycrystalline and belong to the monoclinic crystal system (table 4).

Table 4. XRD data of the Co(II), Cu(II), and Zn(II) complexes.

Parameters	Co(II) complex	Cu(II) complex	Zn(II) complex
E.F	$C_{10}H_{18}N_6CoCl_2O_2$	$C_{10}H_{18}N_6CuCl_2O_2$	$C_{10}H_{16}N_6ZnCl_2O$
F.W	384.13	388.74	372.57
Crystal System	Monoclinic	Monoclinic	Monoclinic
a (Å)	14.22	18.06	11.27
b (Å)	5.94	6.19	23.28
c (Å)	8.20	12.51	26.93
Alfa (°)	90.00	90.00	90.00
Beta(°)	95.88	107.92	108.05
gamma(°)	90.00	90.00	90.00
Particle Size (nm)	119	88	175
V.U.C (Å3)	690	1332	6724

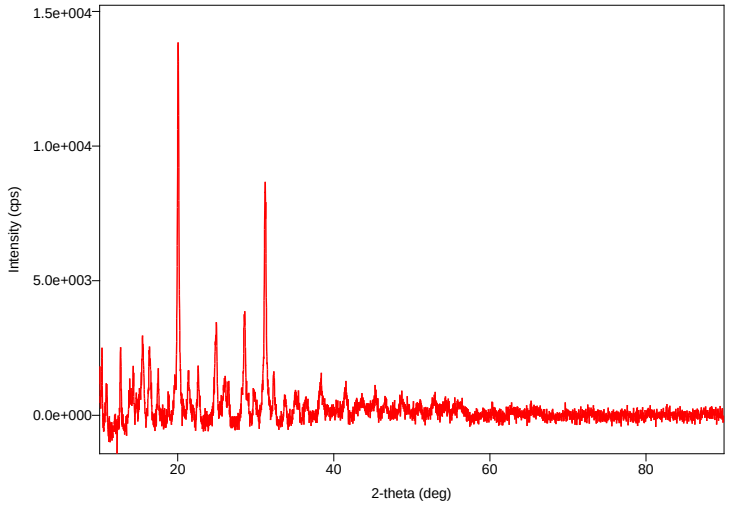

Figure 9. X-ray powder diffraction (XRD) pattern of Cu(II) complex.

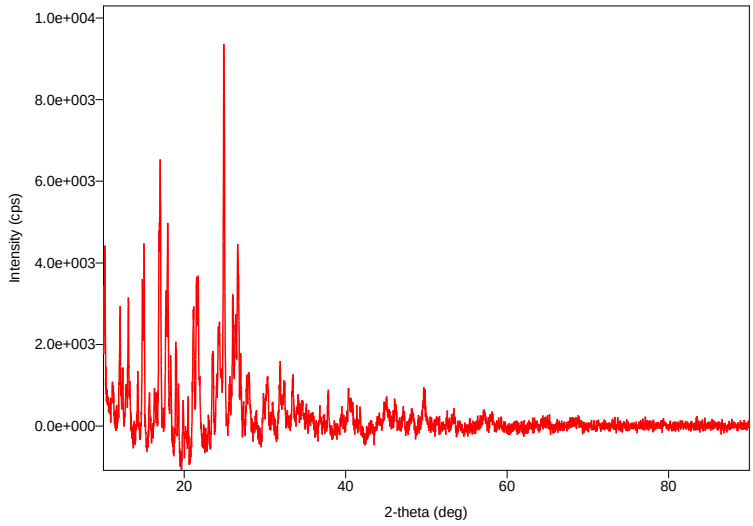

Figure 10. X-ray powder diffraction (XRD) pattern of Zn(II) complex.

Preprints (www.preprints.org) | NOT PEER-REVIEWED | Posted: 19 December 2022 doi:10.20944/preprints202212.0329.v1

3.8. Scanning Electron Microscopy (SEM)

The morphological characteristics of the three complexes synthesized were analyzed by SEM, as shown in (Figure 11. (a), (b), and (c)). The morphology of the Co(II) complex synthesized is consistent with spherical particles. On the other hand, herbal assembly and cluster slice morphology for Cu(II) and Zn(II) compounds, respectively.

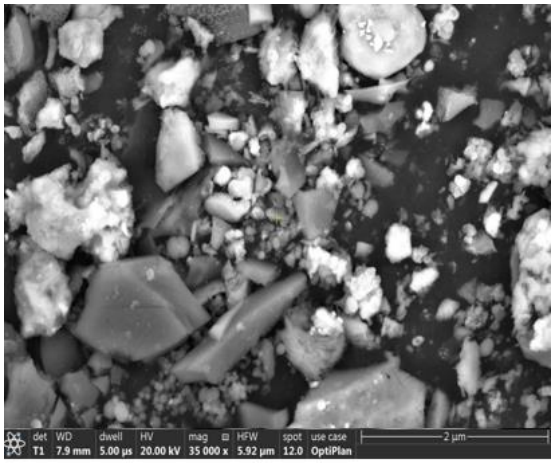

Figure 11. (a). SEM of Co(II) complex.

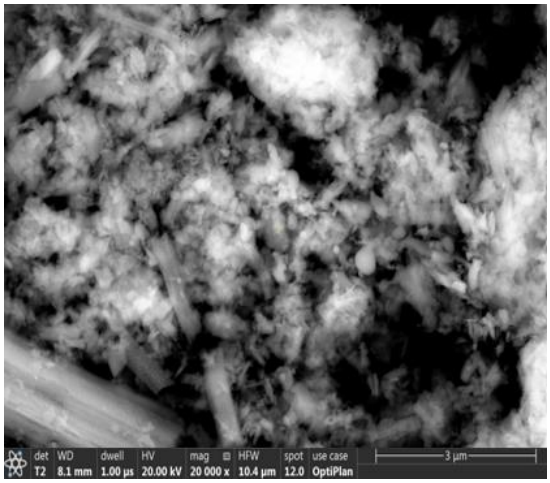

(b). SEM of Cu(II) complex.

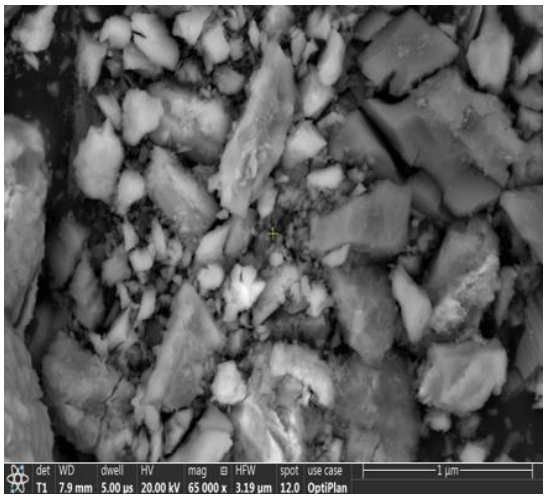

(c). SEM of Zn(II) complex.

3.9. Antimicrobial and Antioxidant Assays

Preprints (www.preprints.org) | NOT PEER-REVIEWED | Posted: 19 December 2022 doi:10.20944/preprints202212.0329.v1

The antimicrobial results summarized in (table 5). The Cu(II) complex and Co(II) complex have the most important effect. They showed a qualitative antibacterial effect with an inhibitory zone ranging between 1cm and 2.5cm for Gram -positive strains like *Staphylococcus aureus* and *Micrococcus luteus* and between 1.2cm and 1.4cm for Gram-negative strains. The tested compounds have an antifungal effect against *Candida albicans* with a maximum inhibitory zone of 2.5cm. As summarized in table 5, the results demonstrated a high antioxidant potential for the Zn(II) complex with a DPPH scavenging of 91.5%, however, the Cu(II) complex was low (16.5%).

Table 5. Antimicrobial and antioxidant effects. (Inhibitory zone expressed in cm ±SD).

	Antimicrobial					Antioxidant
	S1	**S4**	**S5**	**S10**	9C	
Co(II) complex	**2.55**$^{\pm 0.07}$	**1.45**$^{\pm 0.07}$	**1.45**$^{\pm 0.07}$	1.00$^{\pm 0.14}$	**2.35**$^{\pm 0.07}$	0$^{\pm 00}$
Cu(II) complex	**1.5**$^{\pm 0.07}$	1.25$^{\pm 0.07}$	1.00$^{\pm 0.07}$	1.5 $^{\pm 0.14}$	**1.5±0.21**	16.5$^{\pm 2.12}$
Zn(II) complex	**1.6**$^{\pm 0.14}$	1$^{\pm 0.14}$	1.2$^{\pm 00}$	1.3$^{\pm 0.07}$	0$^{\pm 00}$	**91.5**$^{\pm 9.19}$

SD: Standard Deviation; ND: Not Determined.

3.10. In Silico Docking Study

In order to explore potential novel antibacterial compounds, we can study one of the enzymes that contribute to this potential property which is the tyrosyl-tRNA synthetase. It is among the aminoacyl-tRNA synthetases (aaRSs) and is in charge of the catalysis of the covalent bond of amino acids to their corresponding tRNA to make charged tRNA. Therefore, aaRSs inhibition affects the growth of the cell owing to their role in the process of protein biosynthesis. We have to notice that the complex can be degraded in the medium, and the antimicrobial effect can be also due to the interaction of the individual components with the enzyme.

To explore the possible antibacterial activity of the compounds against pathogenic species, docking of the compounds was achieved with the catalytic site of TyrRS from S. aureus built from the structure TyrRS receptor (pdb: 1JIJ). The three compounds showed different values of binding energies with the TyrRS model (Table 6). The results showed that all compounds have good values of binding energy (7.2-7.9kcal mol^{-1}). The data of docking presented that all compounds fit very well in the catalytic pockets of the proteins of the receptor.

The most potent compound Co(II) represented appropriate interactions with different residues of tyrosyl-tRNA synthetase and the results are revealed in Figure 12. The obtained results (figure (12), Table 6) describe that the compound Co(II) having the potent inhibitory activity occupies perfectly the catalytic site of Tyrosyl-tRNA synthetase with a value for the binding energy of −7.2kcal mol^{-1}. Co(II) complex shows four hydrogen bonds, two between the hydrogens of the water molecule attached to the Co metal with Asp195, and two hydrogen bonds between the hydrogens of the two NH_2 attached to the metal with Asp40. The rings of the ligand show π-cation interaction with His50 and π- π, T-shaped interaction with Gly38. It shows Van der Waals interactions with the amino acids of the active site: Asp 80, His47, Lys84, Thr42, Gln196, Ala39, Gln174, Leu70, and Tyr170. These interactions contribute to the stabilization of the complex and suggest that it is involved in its inhibitory effect. These interactions with His47, Ala39, Gln174, Leu70, and Tyr170 are common to the catalytic sites found in compounds having antimicrobial activity [40]. This suggests that they contribute to this property.

Preprints (www.preprints.org) | NOT PEER-REVIEWED | Posted: 19 December 2022 doi:10.20944/preprints202212.0329.v1

Table 6. Docking binding energy (kcal mol^{-1}) of the complexes into the active site of the TyrRS receptor (PDB: 1JIJ).

Compound	1JIJ
Zn(II) complex	-7.2
Cu(II) complex	-7.9
Co(II) complex	-7.2

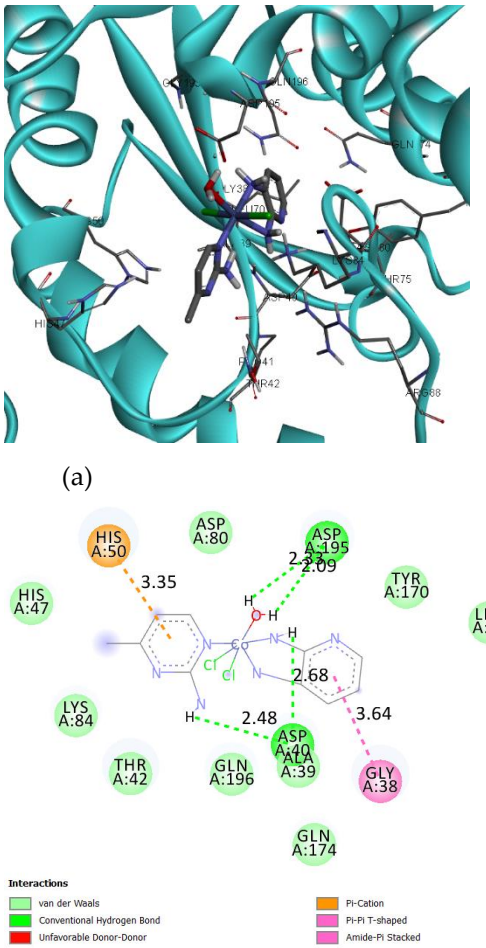

(a)

(b)

Figure 12. (a) Three dimensional (3D) and (b) two-dimensional (2D) interaction of Co(II) complex with the active site of tyrosyl tRNA synthetized (PDB: 1JIJ).

Conclusion

Three new compounds were synthesized. Experimental and theoretical studies were performed to explore their properties:

1. We have successfully prepared the Co(II), Cu(II), and Zn(II) complexes.
2. The solid compounds were isolated and characterized using CHN, FT-IR, UV.*vis*, and magnetic moments.
3. HOMO and LUMO show that the electron distribution is not the same for all molecules and this can lead to different properties.
4. The synthesized of the discussed complexes demonstrated excellent antibacterial and antifungal activities.
5. The results of docking showed that all compounds have good values of binding energy (7.2-7.9kcal mol^{-1}).

6. The data of docking presented that all compounds fit very well in the catalytic pockets of the proteins of the receptor, The Co(II) complex is more active.

In future work, other properties will be studied for these molecules, and advanced in vitro studies will be conducted in order to confirm their potential effects.

Acknowledgments: "The authors extend their appreciation to the Deputyship for Research& Innovation, Ministry of Education, Saudi Arabia, for funding this research work through project number (QU-IF-2-5-4-26289). The authors also thanks to Qassim University for technical support".

References

1. Yu V. Kokunov, Silver complexes with 2-amino-4-methylpyrimidine: Synthesis, crystal structure, and luminescent properties." Russian Journal of Coordination Chemistry 39.8 (2013): 565-570.
2. Navarro, Jorge AR, et al. "Soft functional polynuclear coordination compounds containing pyrimidine bridges." Journal of Solid State Chemistry 178.8 (2005): 2436-2451.
3. Cook, T. R.; Zheng, Y.-R.; Stang, P. J. Metal−organic frameworks and self-assembled supramolecular coordination complexes: comparing and contrasting the design, synthesis, and functionality of metal−organic materials. Chem. Rev.113 (2013) 734−777.
4. Griffin, ScottáT, and RobináD Rogers. "Simple routes to supramolecular squares with ligand corners: 1: 1 Ag I: pyrimidine cationic tetranuclear assemblies." Chemical Communications 2 (1998): 215-216.
5. Pettinari, C.; Tabă caru, A.; Galli, S. Coordination polymers and metal−organic frameworks based on poly (pyrazole)-containing ligands. Coord. Chem. Rev. 307 (2016) 1−31.
6. Ye, Y.; Xiong, S.; Wu, X.; Zhang, L.; Li, Z.; Wang, L.; Ma, X.; Chen, Q.-H.; Zhang, Z.; Xiang, S. Microporous Metal−Organic Framework Stabilized by Balanced Multiple Host−Couteranion Hydrogen-Bonding Interactions for High-Density CO2 Capture at Ambient Conditions. Inorg. Chem. 55 (2016) 292−299.
7. Shahbazi, M.; Mehrzad, F.; Mirzaei, M.; Eshtiagh-Hosseini, H.; Mague, J. T.; Ardalani, M.; Shamsipur, M. Synthesis, single crystal X-ray characterization, and solution studies of Zn (II)-, Cu (II)-, Ag (I)- and Ni (II)-pyridine-2, 6-dipicolinate N-oxide complexes with different topologies and coordination modes. Inorg. Chim. Acta. 458 (2017) 84−96.
8. Tripti Mandal, Arka Dey, Saikat Kumar Seth, Joaquín Ortega-Castro, Arnold L. Rheingold, Partha Pratim Ray, Antonio Frontera, Subrata Mukhopadhyay, Influence of 2-Amino-4-methylpyridine and 2-Aminopyrimidine Ligands on the Malonic Acid-Cu(II) System: Insights through Supramolecular Interactions and Photoresponse Properties, ACS Omega 5 (2020) 460−470.
9. C. Yenikaya, M. Sarı, M. Bülbül, H. İlkimen, H. Çelik, O. Büyükgüngör, Synthesis, characterization and antiglaucoma activity of a novel proton transfer compound and a mixed-ligand Zn(II) complex, Bioorg. Med. Chem. 18 (2010) 930–938.
10. H. Fuhrmann, S. Brenner, P. Arndt, R. Kempe, Octahedral group 4 metal complexes that contain amine, amido, and aminopyridinato ligands: synthesis, structure, and application in α-olefin oligo- and polymerization, Inorg. Chem. 35 (1996) 6742-6745.
11. B. K. London, M. O. F. Claville, S. Babu, F. R. Fronczek, R. M. Uppu, A co-crystal of nona-hydrated disodium(II) with mixed anions from m-chlorobenzoic acid and furosemide, Acta Cryst. E71, (2015) 1266–1269.
12. C. Yenikaya, N. Büyükkıdan, M Sarı, R. Keşli, H. İlkimen, M. Bülbül, O. Büyükgüngör, Synthesis, characterization, and biological evaluation of Cu(II) complexes with the proton transfer salt of 2,6-pyridinedicarboxylic acid and 2- amino-4-methylpyridine, J. Coord. Chem. 64 (2011) 3353–3365.
13. S. Mistri, E. Zangrando, S. C. Manna, Cu(II) complexes of pyridine-2,6-dicarboxylate and N-donor neutral ligands: Synthesis, crystal structure, thermal behavior, DFT calculation and effect of aromatic compounds on their fluorescence, Inorg. Chim. Acta. 405 (2013) 331–338.
14. C. Yenikaya, M. Poyraz, M. Sarı, F. Demirci, H. İlkimen, O. Büyükgüngör, Synthesis, characterization and biological evaluation of a novel Cu(II) complex with the mixed ligands 2,6-pyridinedicarboxylic acid and 2-aminopyridine, Polyhedron. 28 (2009) 3526–3532.
15. Ilkimen, Halil. "Synthesis and characterization of mixed ligand Cu (II) complexes of 2-methoxy-5-sulfamoylbenzoic acid and 2-aminopyridine derivatives." Macedonian Journal of Chemistry and Chemical Engineering 38.1 (2019): 13-17.
16. R. K. Poddar, U. Agarwala, Reactions of Ru(PPh3)2Cl2 and [Ru(AsPh3)2Cl2]2 with various donor molecules, J. Inorg. Nucl. Chem. 35 (1973) 3769–3779.
17. A. G. Raso, J. J. Fiol, A. L. Zafra, A. Cabrero, I. Mata, E. Molins, Crystal structures of the N-salicylidene–Lserinatoaquacopper(II) monohydrate and its ternary derivative with 2-aminopyridine, Polyhedron. 18 (1999) 871–878.
18. Al-Fakeh, Maged S., et al. "Synthesis, Characterization, and Antimicrobial of MnO and CdO Nanoparticles by Using a Calcination Method." Coatings 12.2 (2022): 215.
19. Abdelkarim Mahdhi , Nadia Leban , Ibtissem Chakroun , Mohamed Aymen Chaouch , Jawhar Hafsa , Kais Fdhila , Kacem Mahdouani , Hatem Majdoub, Extracellular polysaccharide derived from potential probiotic strain with antioxidant and antibacterial activities as a prebiotic agent to control pathogenic bacterial biofilm formation. Microbial Pathogenesis. 109 (2014) 220.
20. Dbeibia, Amal, et al. "Control of Staphylococcus aureus methicillin resistant isolated from auricular infections using aqueous and methanolic extracts of Ephedra alata." Saudi Journal of Biological Sciences 29.2 (2022) 1021-1028.
21. M.J. Frisch, G.W. Trucks, H.B. Schlegel, G.E. Scuseria, M.A. Robb, J.R. Cheeseman, J.A. Montgomery Jr., T.K.K.N. Vreven, K.N. Kudin, J.C. Burant, J.M. Millam, Gaussian 09, Revision D.01, Gaussian, Inc., Wallingford CT, 2013.

22. Morris, G.M.; Huey, R.; Olson, A.J. Using AutoDock for ligand-receptor docking. Curr. Protoc. Bioinform. 24 (2008) 8–14.
23. Trott, O.; Olson, A.J. AutoDock Vina: Improving the speed and accuracy of docking with a new scoring function, efficient optimization, and multithreading. J. Comput. Chem. 31 (2010) 455–461.
24. BIOVIA, Dassault Systèmes. "Discovery studio visualizer, v16. 1.0. 15350." San Diego: Dassault Systèmes (2015).
25. Sujin P. Jose and S. Mohan, "Vibrational Spectra and Normal Co-Ordinate Analysis of 2-Aminopyridine and 2-Amino Picoline," Spectrochimica Acta - Part A: Molecular and Biomolecular Spectroscopy. 64. 1(2006) 240–45.
26. Amah Colette et al., "Synthesis , Crystal Structure , and Antimicrobial Properties of a Novel 1-D Cobalt Coordination Polymer with Dicyanamide and 2-Aminopyridine," International Journal of Inorganic Chemistry.2015 (2015) 9-12.
27. Al-Fakeh, Maged S., Gadah A. Allazzam, and Naeema H. Yarkandi. "Ni (II), Cu (II), Mn (II), and Fe (II) Metal Complexes Containing 1, 3-Bis (diphenylphosphino) propane and Pyridine Derivative: Synthesis, Characterization, and Antimicrobial Activity." International Journal of Biomaterials 2021 (2021) 1-12..
28. Anita Raducka, Agnieszka Czylkowska, Katarzyna Gobis, Kamila Czarnecka, Paweł Szyma ´nski and Marcin Swi ¸atkowski, Characterization of Metal-Bound Benzimidazole Derivatives, Effects on Tumor Cells of Lung Cancer, Materials. 14 (2021) 2958.
29. Al-Fakeh, Maged S. "Synthesis, thermal stability and kinetic studies of copper (II) and cobalt (II) complexes derived from 4-aminobenzohydrazide and 2-mercaptobenzothiazole." European Chemical Bulletin. 9.12 (2020) 403-409.
30. Aref A. M. Aly, Mahmoud A. Ghandour, Maged S.Al-Fakeh, Synthesis and characterization of transition metal coordination polymers derived from 1,4- Benzene- dicarboxylic acid and Azoles, 36 (2012), 69 -79. Turkish Journal of Chemistry.
31. Kevin W. Wellington,b Perry T. Kaye,a and Gareth M. Watkin, Designer ligands. Part 14. Novel Mn(lI), Ni(II) and Zn(II) complexes of benzamide- and biphenyl-derived ligands, ARKIVOC (2008) 248-264.
32. Mahmoud A. Ghandour, Aref A. M. Aly, Maged S.Al-Fakeh, Synthesis and characterization of Cu(II), Cd(II) and Pb(II) coordination polymers derived from 1,4- benzene- and 1,1'- ferrocenedicarboxylate and 2- aminobenzothiazole. J. Indian Chem. Soc. 88, 9 (2011)1633-1638.
33. Maged S. Al-Fakeh, Synthesis and characterization of coordination polymers of 1, 3-di (4-pyridyl)-propane and 2-aminobenzothiazole with Mn(II), Co(II), Cu(II) and Ni(II) ions. Journal of Chemical and Pharmaceutical Research. 10.2 (2018) 77-83.
34. Al-Fakeh, M., Alsaedi, R. Synthesis, Characterization and Antimicrobial Activity of CoO Nanoparticles from a Co (II) Complex Derived from Polyvinyl Alcohol and Aminobenzoic Acid Derivative. The Scientific World Journal. 2021 (2021) 1-11.
35. Aly, A. A., Ghandour, M. A., Abu-Zied, B. M., & Al-Fakeh, M. S. Synthesis, properties and environmentally important nanostructured and antimicrobial supramolecular coordination polymers containing 5-(3-pyridyl)-1, 3, 4-oxadiazole-2-thiol and benzimidazole. J Environ Anal Toxicol. 2 (2012) 2-7.
36. Al-Fakeh, M., and F. Alminderej. "New method for the preparation and biological activity of CuO nanoparticles from a mixed PVA and 2-Aminobenzothiazole complex." International Journal of Chem.Tech Research. 11.05 (2018) 442-449.
37. M.M. El-ajaily, S.F. Ben-Gweirif, R.S. El-zweay and A. A. Maihub, Synthesis Of Some Mixed Ligand Complexes Derived From Catechol And 2- Aminopyridine And Their Biological Activity, Journal of Sebha University-(Pure and Applied Sciences). 6.3 (2007) 5.
38. Uçar, İbrahim, et al. "Synthesis, structure, spectroscopic and electrochemical properties of (2-amino-4-methylpyrimidine)-(pyridine-2, 6-dicarboxylato) copper (II) monohydrate." Journal of molecular structure. 834 (2007) 336-344.
39. Mikhail S. Bukharov, Valery G. Shtyrlin, Georgy V. Mamin, Siegfried Stapf, Carlos Mattea, Anvar Sh. Mukhtarov, Nikita Yu. Serov, and Edward M. Gilyazetdinov Inorganic Chemistry. 54 .20 (2015) 9777-9784.
40. Alminderej F, Bakari S, Almundarij TI, Snoussi M, Aouadi K, Kadri A. Antimicrobial and Wound Healing Potential of a New Chemotype from Piper cubeba L. Essential Oil and In Silico Study on S. aureus tyrosyl-tRNA Synthetase Protein. Plants (Basel). Jan 22;10(2) (2021) 205.